Nanoscale Advances

PAPER

View Article Online
View Journal | View Issue

Cite this: *Nanoscale Adv.*, 2019, **1**, 2606

Growth of vertical heterostructures based on orthorhombic SnSe/hexagonal In_2Se_3 for high-performance photodetectors†

Xuan-Ze Li,[ab] Yi-Fan Wang,[ab] Jing Xia*[a] and Xiang-Min Meng *[a]

Vertical heterostructures based on two-dimensional (2D) layered materials are ideal platforms for electronic structure engineering and novel device applications. However, most of the current heterostructures focus on layered crystals with a similar lattice. In addition, the heterostructures made by 2D materials with different structures are rarely investigated. In this study, we successfully fabricated vertical heterostructures by combining orthorhombic SnSe/hexagonal In_2Se_3 vertical heterostructures using a two-step physical vapor deposition (PVD) method. Structural characterization reveals that the heterostructures are formed of vertically stacked SnSe on the top of the In_2Se_3 film, and vertical heterostructures possess high quality, where In_2Se_3 exposed surface is the (0001) plane and SnSe prefers growing along the [100] direction. Raman maps confirm the precise spatial modulation of the as-grown SnSe/In_2Se_3 heterostructures. In addition, high-performance photodetectors based on the vertical heterostructures were fabricated directly on the substrate, which showed a broadband response, reversibility and stability. Compared with the dark current, the device demonstrated one order magnification of photocurrent, about 186 nA, under 405 nm laser illumination and power of 1.5 mW. Moreover, the device shows an obvious increase in the photocurrent intensity with the changing incident laser power, where $I_{ph} \propto P^{0.7}$. Also, the device demonstrated a high responsivity of up to 350 mA W^{-1} and a fast response time of about 139 ms. This study broadens the horizon for the synthesis and application of vertical heterostructures based on 2D layered materials with different structures and further develops exciting technologies beyond the reach of the existing materials.

Received 25th February 2019
Accepted 13th May 2019

DOI: 10.1039/c9na00120d

rsc.li/nanoscale-advances

Introduction

Two-dimensional (2D) materials provide a wide range of basic building blocks with distinct optical and electrical properties, which can modulate electrical bands structures[1–6] and improve optoelectronic properties.[7–11] Furthermore, heterostructures can offer a various playground for investigating basic physical and chemical issues.[12–18] Tin(II) selenide (SnSe), as a member of IVA–VIA group, is a stable and distinctive 2D material consisting of earth abundant elements. In addition, SnSe exhibits some novel properties, especially its high thermoelectric performance with a ZT (figure of merit) value of 2.6 and 2.3 at 923 K along the *b* and *c* directions, respectively,[19,20] which provides a practical way to solve the global energy demands, together with the negative impacts resulting from the combustion of fossil fuels.[21]

Moreover, SnSe is an attractive binary p-type semiconductor material, with an indirect band gap at 0.90 eV and a direct band gap at 1.30 eV,[22,23] which has a wide range of potential applications in infrared optoelectronic devices and photoelectric detectors.[24–27] However, the onefold bandgap restricts the application fields of SnSe and a heterostructure based on SnSe is needed. Currently, most of heterostructures focus on layered crystals with a similar lattice.[28–32] Tongay reported the chemical vapor deposition and growth dynamics of highly anisotropic 2D lateral heterojunctions between pseudo-1D ReS_2 and isotropic WS_2 for the first time.[33] They found the degree of anisotropy of ReS_2 on WS_2 largely depends on the domain size, which is a significant leap forward for the large-scale nanomanufacturing of anisotropic systems. Furthermore, He *et al.* epitaxially synthesized lateral NbS_2–WS_2 heterostructure *via*

---

[a] *Key Laboratory of Photochemical Conversion and Optoelectronic Materials, Technical Institute of Physics and Chemistry, Chinese Academy of Sciences, Beijing, 100190, P. R. China. E-mail: mengxaingmin@mail.ipc.ac.cn; xiajing@mail.ipc.ac.cn*

[b] *Centre of Material Science and Optoelectronic Engineering, University of Chinese Academy of Science, Beijing, 10049, P. R. China*

† Electronic supplementary information (ESI) available: Optical images of the In_2Se_3 sample on mica substrate. AFM image and height profile of the In_2Se_3 film. Optical images of the SnSe/In_2Se_3 vertical van der Waals heterostructure. XRD pattern of the empty mica substrate and the as-grown SnSe/In_2Se_3. Potential profile image of In_2Se_3 film and the SnSe nanoplate. Pixel intensity profile of In_2Se_3 and SnSe on the heterostructure. Bright field TEM (BFTEM) image of In_2Se_3. High resolution TEM (HRTEM) image of the In_2Se_3 sample and the corresponding SAED pattern. Dark field (DF) STEM image of In_2Se_3. Elements maps of In_2Se_3 sample showing spatial distribution of Se and In. *I–V* curves of the devices based on the SnSe nanosheet and SnSe/In_2Se_3 heterostructure in the dark and the detail *I–V* characteristic of heterostructure shown in inserted diagram. See DOI: 10.1039/c9na00120d

a two-step CVD method and the FET based on the heterostructure possessed a well-defined rectification.[34] Heterostructures made by 2D materials with different structures are rarely investigated today. Hence, hexagonal In_2Se_3 comes into our sight. In_2Se_3 is an interesting semiconductor of the $A_2^{III}B_3^{VI}$ family with double layers of nonmetal atoms and each unit cell consists of [Se–In–Se–In–Se] sheets stacked together through the Se atoms along the *c*-axis.[35–40] Recently, the n-type In_2Se_3 is becoming one of the promising materials for detecting visible light due to its direct and narrow band gap (1.95 eV) and high absorption coefficient in the visible range.[41–46]

In this study, by combining orthorhombic SnSe and hexagonal In_2Se_3, a new vertical heterostructure was prepared *via* a simple two-step PVD method. Then, the characteristics of morphology, crystalline phase and microstructure of the vertical heterostructure samples were investigated in detail, and the results showed the orthorhombic SnSe nanoplates randomly grown on the top of the hexagonal In_2Se_3 film with an exposing (100) plane. The samples possess excellent Raman properties, and Raman intensity mappings further confirm the successful achievement of the SnSe/In_2Se_3 vertical heterostructures. The photoelectric devices based on the SnSe/In_2Se_3 vertical heterostructures were directly fabricated. The devices demonstrate a dramatic current increase with lower power laser illumination (70 nA at 30 μW 405 nm laser), high responsivity (R) up to 350 mA W^{-1} and fast photoresponse with 139 ms. This study creates a new avenue for the realization of novel 2D electronic and optoelectronic devices, and more importantly, develops exciting technologies beyond the reach of the existing materials.

Experimental section

Growth of hexagonal In_2Se_3 film

Hexagonal In_2Se_3 film was prepared on fluorochrome mica substrates *via* a simple physical vapor deposition (PVD) method. The preparation process occurred in a single temperature zone tube furnace. About 0.1 g In_2Se_3 (99.999%, Alfa) powder and 1 g Se (99.999%, Alfa) powder were loaded in two Al_2O_3 boats. Then, the In_2Se_3 powder was placed at the heating centre of a quartz tube furnace and the Se powder was put at the upstream of the tube furnace. Two pieces of newly cleaved mica substrates were positioned at the downstream of the tube furnace around 10 cm away from the In_2Se_3 precursor. The tube furnace was pumped down first, and then filled with high-purity Ar gas to the chamber pressure of about 10 Torr. Sixty sccm Ar was used for the growth of the In_2Se_3 film. The temperature of the heating zone increased gradually to 850 °C from room temperature in 35 min and remained for 2 min. After the reaction, the furnace was cooled down to room temperature naturally.

Synthesis of SnSe/In_2Se_3 vertical heterostructures

The SnSe/In_2Se_3 heterostructures were synthesized by directly depositing SnSe on the pre-fabricated In_2Se_3 film in a horizontal tube furnace. In the experiment, about 0.1 g SnSe powder (99.999%, Alfa) was kept at the heating center and the mica sheets with In_2Se_3 film were placed at the downstream of the tube furnace about 8 cm away from the SnSe powder. The tube furnace chamber was evacuated, and then filled with high-purity Ar to atmospheric pressure. The growth temperature was 800 °C and kept for 5 min with a 60 sccm Ar flow. After the growth, the furnace was cooled down to room temperature naturally.

Characterization

The morphologies of the hexagonal In_2Se_3 film and SnSe/In_2Se_3 vertical heterostructures were investigated using an inverted optical microscope (Nikon Inverted Microscope Eclipse Ti-U with a Nikon Digital Sight) and a Hitachi S-4800 field-emission scanning electron microscope (SEM).

The thickness of the samples was confirmed by an atomic force microscope (AFM) Bruker Multimode 8.

X-ray diffraction (XRD) patterns were obtained by a powder X-ray diffractometer (Bruker D8 Focus) with Cu-Kα radiation ($\lambda = 1.5418$ Å).

The microstructure and the elemental composition of the as-grown samples were investigated using a JEOL JEM-2100F field-emission transmission electron microscope (TEM) equipped with an energy dispersive X-ray spectroscopy (EDS).

The Raman properties of the SnSe/In_2Se_3 vertical heterostructures were identified using a confocal Raman microscope (Renishaw InVia) with a 532 nm laser.

Device fabrication and measurements

Photodetectors based on the SnSe/In_2Se_3 vertical heterostructures and SnSe nanoplates were directly fabricated on the mica substrates. In brief, Au electrodes were deposited on the surface of the as-prepared samples *via* thermal evaporation using Cu grids as the shadow mask. Then, the devices were annealed at 200 °C for 2 hours in Ar atmosphere to improve the contact between the electrodes and the heterostructures. The Photoresponse property of the device was investigated using a Keithley-4200 SCS semiconductor parameter analyzer and a cryogenic probe station. Four different incident lasers (685 nm, 532 nm, 450 nm and 405 nm) were adopted for the illumination.

Results and discussion

The SnSe/In_2Se_3 vertical heterostructures were synthesised using a simple two-step PVD technology, and the preparation process is displayed in Fig. 1a. The SEM image and optical characteristics in Fig. 1b and S1† confirm the formation of a uniform In_2Se_3 film on the mica substrate and the thickness of the film was determined to be about 16 nm (Fig. S1b†). In the second growth step, the SnSe nanoplates were found to have grown randomly on the as-grown In_2Se_3 film (Fig. S1c and d†) and showed a rhombic shape with a side length of about 12 μm and a thickness of 48 nm (Fig. 1c and d). The crystalline phase of the SnSe/In_2Se_3 heterostructure was then investigated using XRD characterization, as displayed in Fig. 1e. Compared with the reference XRD patterns of In_2Se_3 (PDF 34-0455) and SnSe

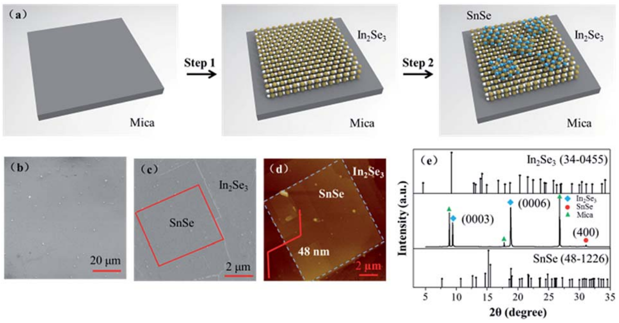

Fig. 1 (a) Schematic illustrating the preparation process of the vertical heterostructure. (b and c) SEM images of the In_2Se_3 film and SnSe/In_2Se_3 vertical heterostructures. (d) AFM image and height profile of the SnSe/In_2Se_3 vertical heterostructure. (e) XRD pattern of the as-grown SnSe/In_2Se_3 and the reference XRD data of SnSe and In_2Se_3.

(PDF 48-1226), the strong peaks located at 9.4° and 18.8° can be indexed to the (0003) and (0006) planes of the hexagonal phase In_2Se_3, while the weak diffraction peak at 31.08° can be ascribed to the (400) plane of the orthorhombic SnSe. Other obvious diffraction peaks come from the (0001) planes of the fluorophlogopite mica substrate (Fig. S2†).

The microstructure of the SnSe/In_2Se_3 vertical heterostructure was also investigated using a transmission electron microscope equipped with EDS as exhibited in Fig. 2. The low-magnification TEM image in Fig. 2a shows a vertical heterostructure composed of SnSe nanoplates and In_2Se_3 film at the bottom. The atomic ratio of Se, In and Sn is confirmed to be about 4 : 2 : 1 (Fig. 2b), matching well with the stoichiometric ratio of a mixture of SnSe and In_2Se_3. And cuprum in EDS spectrum is from the copper grid. Fig. 2c and e are the high-resolution TEM (HRTEM) images of SnSe and In_2Se_3 from the heterostructure sample, respectively. The lattice fringes measured from the HRTEM images (Fig. 2c and e) are about 0.35 nm and 0.31 nm (Fig. S4†), which match well with the (10–10) plane of the hexagonal In_2Se_3 and the (011) plane of the orthorhombic SnSe, respectively. The corresponding SAED images of In_2Se_3 and the heterostructure sample are exhibited in Fig. 2d and f. A set of well-arranged diffraction spots confirm the good quality and single crystallinity of the heterostructure. To study the spatial elemental distribution of the sample, EDS elemental mappings and bright field scanning TEM (STEM) image of the vertical heterostructure were then recorded, as displayed in Fig. 2g–j. It can be obviously seen that the In element has a uniform intensity distribution, while Sn is only distributed around the right region in the bright field STEM image of Fig. 2g, indicating the successful fabrication of the vertical heterostructure based on orthorhombic SnSe and hexagonal In_2Se_3.

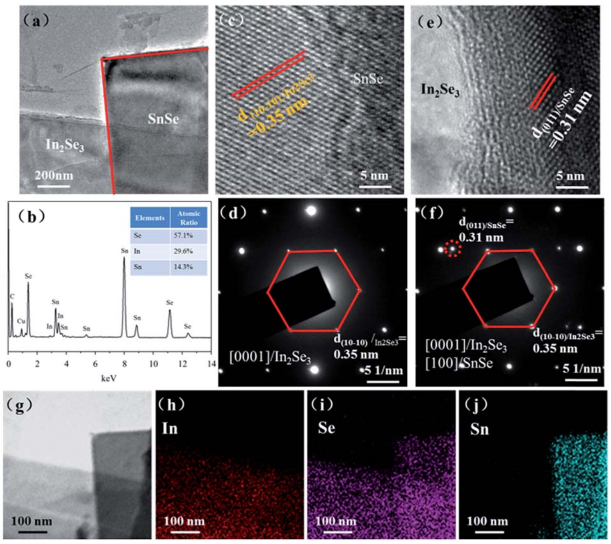

Fig. 2 (a) Bright field TEM image of the SnSe/In_2Se_3 vertical heterostructure sample. (b) EDS spectrum of the heterostructure sample. (c and d) HRTEM image and SAED pattern of the In_2Se_3 film in the heterostructure sample. (e and f) HRTEM image and SAED pattern of SnSe in the heterostructure sample. (g) Bright field STEM image of the SnSe/In_2Se_3 heterostructure sample. (h–j) Element mappings of the vertical heterostructure.

The optical properties of the as-prepared SnSe/In_2Se_3 vertical heterostructures were studied in detail using Raman spectroscopy. The typical Raman spectra of the In_2Se_3 film, the SnSe/In_2Se_3 heterostructure, and SnSe are shown in Fig. 3a. Compared with the Raman spectrum of the single SnSe and In_2Se_3, it can be clearly seen that the heterostructure possesses three strong peaks at 69 cm^{-1}, 148 cm^{-1} and 103 cm^{-1}, which can be ascribed to the A_g vibration modes of rhombic SnSe and the interlayer vibration mode of γ-In_2Se_3, respectively. In addition, the Raman intensity mappings of 69 cm^{-1} and 103 cm^{-1} modes of the heterostructure were also recorded, as shown in Fig. 3c and d, respectively. It can be observed that the Raman signal of SnSe exists only in the center of the image, while the In_2Se_3 Raman signal distributes throughout the whole image, which further confirms the successful fabrication of the SnSe/In_2Se_3 vertical heterostructures.

Furthermore, the optoelectronic property of the SnSe/In_2Se_3 vertical heterostructure was also investigated. Photodetectors

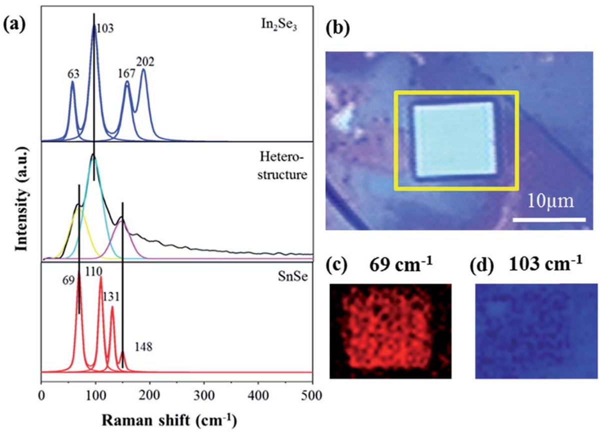

Fig. 3 (a) Raman spectra of the In_2Se_3 film, the SnSe/In_2Se_3 vertical heterostructure, and SnSe. (b) Optical image of a vertical heterostructure. (c and d) Raman intensity mappings of the Raman modes at 69 cm^{-1} and 103 cm^{-1} of the heterostructure marked in (b).

based on the vertical heterostructure were directly fabricated on the mica substrate and the schematic model is displayed in Fig. 4a. Compared with the properties of the device based on the SnSe nanosheet, the heterostructure possesses a small dark current, about 15 nA, shown in Fig. S7,† suggesting that the SnSe/In_2Se_3 vertical heterostructure is more suitable for light detection. Simultaneously, it can be easily seen that the *I–V* curves show an obvious asymmetric characteristic (Fig. S7†), which indicates the formation of a p–n junction in the SnSe/In_2Se_3 vertical heterostructure and the forward bias is utilized to learn the photoelectronic properties of the heterostructure. Fig. 4b shows the *I–V* curves of the device in the dark and under different laser illumination with the same laser power. Obviously, the current declines as the laser wavelength increases and the current reaches the maximum of 70 nA under 405 nm laser illumination and 5 V bias (Fig. 4b). The broadband response of the device is attributed to the band gap modulation of SnSe and In_2Se_3. Next, the 405 nm laser was used to investigate the photoelectronic properties in the follow-up experiments due to the best photoresponse. Fig. 4c shows the *I–V* curves of the device under the 405 nm laser illumination with different powers from 30 μW to 1.5 mW. The linear *I–V* curves imply that ohmic contacts have formed between the Au electrode and the heterostructure. A pronounced increase in the current is observed when the device is illuminated with lower laser power and the photocurrent ($I_{\text{ph}} = I_{\text{illumination}} - I_{\text{dark}}$) exhibits one order of magnitude larger than the dark current when the laser power is 1.5 mW, suggesting a strong photoresponse of the device. In Fig. 4d, the photocurrent as a function of the light intensity was plotted. By fitting the experimental data, it is found that the photocurrent can be expressed by a power law equation $I_{\text{ph}} \propto P^{0.7}$, where *P* is the light intensity,[47] indicating good absorption and response to the incident laser. One critical parameter to estimate the performance of the photodetector is photoresponsivity (*R*), which can be defined by $R = I_{\text{ph}}/PS$, where *S* is the effective illumination area of the photodetector.[47] For our device, the effective illumination area is about 144 μm^2 and *R* is calculated to be 180 mA W^{-1}–350 mA W^{-1}, which is comparable with other heterostructure photodetectors.[12,48–50]

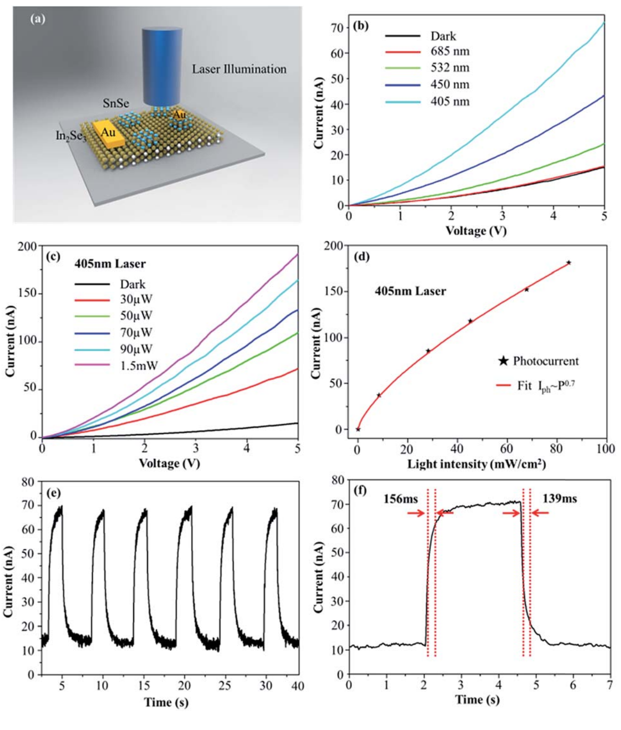

Fig. 4 (a) Schematic of the photodetector based on the SnSe/In_2Se_3 vertical heterostructure. (b) *I–V* curves of the devices in the dark and under different laser illumination with same incident laser power 30 μW. (c) *I–V* curves of the device *via* 405 nm laser illumination with different laser power. (d) Light intensity dependence of the photocurrent at 5 V bias. (e) Time-resolved photoresponse of the device at 5 V bias and 30 μW. (f) A single cycle response to laser on and off.

Another important parameter for evaluating the performance of the photodetector is the response time. For revealing the response speed, the time-resolved photo-current curve of the device was investigated as shown in Fig. 4e. Under the laser illumination, the current of the device rises drastically and the photo-current increases three times with 5 V bias and a laser power of about 10 mW cm^{-2}. After several circles, the device still exhibited a rapid and stable response to the laser illumination. For further evaluating the response rate, we used a chopper with high frequencies to switch the laser. As shown in Fig. 4f, when the laser illumination is in "on" state, the current increases by more than 90% in 156 ms. Meanwhile, the current declines dramatically by more than 90% in 139 ms when the laser illumination is in "off" state. The good reversibility and stability of the device enable the SnSe/In_2Se_3 vertical heterostructure to be a good building block for high-performance optoelectronic devices.

Conclusions

The vertical heterostructure was built *via* the combination of orthorhombic SnSe and hexagonal In_2Se_3, using a simple two-step PVD technology, where SnSe randomly grew on the top of the In_2Se_3 film. The thicknesses of the two materials were about 48 nm and 16 nm, respectively. The XRD pattern indicates the high crystallinity of the heterostructure, preferentially along the[51] [100] direction (SnSe) and [0001] direction (In_2Se_3). The HRTEM and SAED results show that the achieved heterostructure possessed high quality and single crystallinity. Moreover, the Raman studies of the heterostructure well-matched with the characteristic peaks of SnSe and In_2Se_3 and further confirm the relative spatial positions of the two materials in the heterostructure. Furthermore, a two electrode photoresponse device based on the SnSe/In_2Se_3 vertical heterostructure was fabricated. The device shows a broadband response and the photocurrent displays one order magnification compared with the dark current with a 1.5 mW incident laser. Meanwhile, the photocurrent intensity of the device dramatically increased with changing the incident laser power and it is well defined as $I_{\text{ph}} \propto P^{0.7}$, showing good absorption and response to laser illumination. Moreover, the device possessed a high photoresponsivity of up to 350 mA W^{-1} and the response time was about 139 ms, indicating that the SnSe/In_2Se_3 vertical heterostructure had great potential to be applied in the broadband photodetectors field. Also, this study creates a new avenue for the realization of novel 2D electronic and optoelectronic devices, and more importantly, can develop exciting technologies beyond the reach of the existing materials.

Conflicts of interest

There are no conflicts to declare.

Acknowledgements

This study was supported by "Strategic Priority Research Program" of Chinese Academy of Sciences (Grant No. XDA09040203), National Key Basic Research Program of China (973 Program) (Grant No. 2012CB932401) and National Natural Science Foundation of China (Grant No: 11704389).

References

1 T. Roy, M. Tosun, M. Hettick, G. H. Ahn, C. M. Hu and A. Javey, *Appl. Phys. Lett.*, 2016, **108**, 083111.

2 R. D. Westover, G. Mitchson, J. J. Ditto and D. C. Johnson, *Eur. J. Inorg. Chem.*, 2016, 1225–1231.

3 W. Zhou, Y. Guo, J. Liu, F. Q. Wang, X. Li and Q. Wang, *Nanoscale*, 2018, **10**, 13767–13772.

4 F. Withers, O. Del Pozo-Zamudio, A. Mishchenko, A. P. Rooney, A. Gholinia, K. Watanabe, T. Taniguchi, S. J. Haigh, A. K. Geim, A. I. Tartakovskii and K. S. Novoselov, *Nat. Mater.*, 2015, **14**, 301–306.

5 H. C. Diaz, Y. Ma, S. Kolekar, J. Avila, C. Chen, M. C. Asensio and M. Batzill, *2d Mater.*, 2017, **4**, 025094.

6 H. Jin, J. Li, Y. Wei, Y. Dai and H. Guo, *ACS Appl. Mater. Interfaces*, 2018, **10**, 25401–25408.

7 M. Zhao, M. M. Liu, Y. Q. Dong, C. Zou, K. Q. Yang, Y. Yang, L. J. Zhang and S. M. Huang, *J. Mater. Chem. C*, 2016, **4**, 10215–10222.

8 Y. Wen, L. Yin, P. He, Z. Wang, X. Zhang, Q. Wang, T. A. Shifa, K. Xu, F. Wang, X. Zhan, F. Wang, C. Jiang and J. He, *Nano Lett.*, 2016, **16**, 6437–6444.

9 W. Feng, Z. Jin, J. Yuan, J. Zhang, S. Jia, L. Dong, J. Yoon, L. Zhou, R. Vajtai, J. M. Tour, P. M. Ajayan, P. Hu and J. Lou, *2d Mater.*, 2018, **5**, 025008.

10 R. Ai, X. Guan, J. Li, K. Yao, P. Chen, Z. Zhang, X. Duan and X. Duan, *ACS Nano*, 2017, **11**, 3413–3419.

11 D. J. Terry, V. Zolyomi, M. Hamer, A. V. Tyurnina, D. G. Hopkinson, A. M. Rakowski, S. J. Magorrian, N. Clark, Y. M. Andreev, O. Kazakova, K. Novoselov, S. J. Haigh, V. I. Fal'ko and R. Gorbachev, *2d Mater.*, 2018, **5**, 041009.

12 T. Hong, B. Chamlagain, T. J. Wang, H. J. Chuang, Z. X. Zhou and Y. Q. Xu, *Nanoscale*, 2015, **7**, 18537–18541.

13 M. Liu, M. B. Johnston and H. J. Snaith, *Nature*, 2013, **501**, 395–398.

14 H. Chen, X. Wen, J. Zhang, T. Wu, Y. Gong, X. Zhang, J. Yuan, C. Yi, J. Lou, P. M. Ajayan, W. Zhuang, G. Zhang and J. Zheng, *Nat. Commun.*, 2016, **7**, 12512.

15 P. Rivera, J. R. Schaibley, A. M. Jones, J. S. Ross, S. Wu, G. Aivazian, P. Klement, K. Seyler, G. Clark, N. J. Ghimire, J. Yan, D. G. Mandrus, W. Yao and X. Xu, *Nat. Commun.*, 2015, **6**, 7242.

16 A. Dankert and S. P. Dash, *Nat. Commun.*, 2017, **8**, 16093.

17 J. Lee, J. Huang, B. G. Sumpter and M. Yoon, *2d Mater.*, 2017, **4**, 021016.

18 R. Vilaplana, S. G. Parra, A. Jorge-Montero, P. Rodriguez-Hernandez, A. Munoz, D. Errandonea, A. Segura and F. J. Manjon, *Inorg. Chem.*, 2018, **57**, 8241–8252.

19 L. D. Zhao, S. H. Lo, Y. S. Zhang, H. Sun, G. J. Tan, C. Uher, C. Wolverton, V. P. Dravid and M. G. Kanatzidis, *Nature*, 2014, **508**, 373–378.

20 A. T. Duong, V. Q. Nguyen, G. Duvjir, V. T. Duong, S. Kwon, J. Y. Song, J. K. Lee, J. E. Lee, S. Park, T. Min, J. Lee, J. Kim and S. Cho, *Nat. Commun.*, 2016, **7**, 13713.

21 M. Gharsallah, F. Serrano-Sanchez, N. M. Nemes, F. J. Mompean, J. L. Martinez, M. T. Fernandez-Diaz, F. Elhalouani and J. A. Alonso, *Sci. Rep.*, 2016, **6**, 26774.

22 G. S. Shi and E. Kioupakis, *Nano Lett.*, 2015, **15**, 6926–6931.

23 Q. X. Wang, W. Y. Yu, X. N. Fu, C. Qiao, C. X. Xia and Y. Jia, *Phys. Chem. Chem. Phys.*, 2016, **18**, 8158–8164.

24 L. Li, Z. Chen, Y. Hu, X. W. Wang, T. Zhang, W. Chen and Q. B. Wang, *J. Am. Chem. Soc.*, 2013, **135**, 1213–1216.

25 S. Zhao, H. Wang, Y. Zhou, L. Liao, Y. Jiang, X. Yang, G. Chen, M. Lin, Y. Wang, H. Peng and Z. Liu, *Nano Res.*, 2015, **8**, 288–295.

26 D. S. Zheng, H. H. Fang, M. S. Long, F. Wu, P. Wang, F. Gong, X. Wu, J. C. Ho, L. Liao and W. D. Hu, *ACS Nano*, 2018, **12**, 7239–7245.

27 F. K. Butt, M. Mirza, C. B. Cao, F. Idrees, M. Tahir, M. Safdar, Z. Ali, M. Tanveer and I. Aslam, *CrystEngComm*, 2014, **16**, 3470–3473.

28 X. Hong, J. Kim, S.-F. Shi, Y. Zhang, C. Jin, Y. Sun, S. Tongay, J. Wu, Y. Zhang and F. Wang, *Nat. Nanotechnol.*, 2014, **9**, 682–686.

29 X. Huang, M. G. Willinger, H. Fan, Z. L. Xie, L. Wang, A. Klein-Hoffmann, F. Girgsdies, C. S. Lee and X. M. Meng, *Nanoscale*, 2014, **6**, 8787–8795.

30 Y. Jung, J. Shen, Y. Sun and J. J. Cha, *ACS Nano*, 2014, **8**, 9550–9557.

31 K. E. Aretouli, D. Tsoutsou, P. Tsipas, J. Marquez-Velasco, S. A. Giamini, N. Kelaidis, V. Psycharis and A. Dimoulas, *ACS Appl. Mater. Interfaces*, 2016, **8**, 23222–23229.

32 K. Chen, X. Wan, J. Wen, W. Xie, Z. Kang, X. Zeng, H. Chen and J.-B. Xu, *ACS Nano*, 2015, **9**, 9868–9876.

33 B. Chen, K. Wu, A. Suslu, S. Yang, H. Cai, A. Yano, E. Soignard, T. Aoki, K. March, Y. Shen and S. Tongay, *Adv. Mater.*, 2017, **29**, 1701201.

34 Y. Zhang, L. Yin, J. Chu, T. A. Shifa, J. Xia, F. Wang, Y. Wen, X. Zhan, Z. Wang and J. He, *Adv. Mater.*, 2018, **30**, 1803665.

35 W. Feng, F. Gao, Y. Hue, M. Dai, H. Li, L. Wang and P. Hue, *Nanotechnology*, 2018, **29**, 445205.

36 Y. Zhou, D. Wu, Y. H. Zhu, Y. J. Cho, Q. He, X. Yang, K. Herrera, Z. D. Chu, Y. Han, M. C. Downer, H. L. Peng and K. J. Lai, *Nano Lett.*, 2017, **17**, 5508–5513.

37 S. M. Poh, S. J. R. Tan, H. Wang, P. Song, I. H. Abidi, X. Zhao, J. Dan, J. Chen, Z. Luo, S. J. Pennycook, A. H. Castro Neto and K. P. Loh, *Nano Lett.*, 2018, **18**, 6340–6346.

38 M. Lin, D. Wu, Y. Zhou, W. Huang, W. Jiang, W. Zheng, S. Zhao, C. Jin, Y. Guo, H. Peng and Z. Liu, *J. Am. Chem. Soc.*, 2013, **135**, 13274–13277.

39 N. Balakrishnan, E. D. Steer, E. F. Smith, Z. R. Kudrynskyi, Z. D. Kovalyuk, L. Eaves, A. Patane and P. H. Beton, *2d Mater.*, 2018, **5**, 035026.

40 M. Küpers, P. M. Konze, A. Meledin, J. Mayer, U. Englert, M. Wuttig and R. Dronskowski, *Inorg. Chem.*, 2018, **57**, 11775–11781.

41 S. Wan, Y. Li, W. Li, X. Mao, W. Zhu and H. Zeng, *Nanoscale*, 2018, **10**, 14885–14892.

42 D. Wu, A. J. Pak, Y. N. Liu, Y. Zhou, X. Y. Wu, Y. H. Zhu, M. Lin, Y. Han, Y. Ren, H. L. Peng, Y. H. Tsai, G. S. Hwang and K. J. Lai, *Nano Lett.*, 2015, **15**, 8136–8140.

43 H. Peng, C. Xie, D. T. Schoen and Y. Cui, *Nano Lett.*, 2008, **8**, 1511–1516.

44 J. O. Island, S. I. Blanter, M. Buscema, H. S. J. van der Zant and A. Castellanos-Gomez, *Nano Lett.*, 2015, **15**, 7853–7858.

45 C. Cui, W.-J. Hu, X. Yan, C. Addiego, W. Gao, Y. Wang, Z. Wang, L. Li, Y. Cheng, P. Li, X. Zhang, H. N. Alshareef, T. Wu, W. Zhu, X. Pan and L.-J. Li, *Nano Lett.*, 2018, **18**, 1253–1258.

46 W. Feng, F. Gao, Y. Hu, M. Dai, H. Liu, L. Wang and P. Hu, *ACS Appl. Mater. Interfaces*, 2018, **10**, 27584–27588.

47 J. Xia, D. D. Zhu, L. Wang, B. Huang, X. Huang and X. M. Meng, *Adv. Funct. Mater.*, 2015, **25**, 4255–4261.

48 Z. Y. Jia, J. Y. Xiang, F. S. Wen, R. L. Yang, C. X. Hao and Z. Y. Liu, *ACS Appl. Mater. Interfaces*, 2016, **8**, 4781–4788.

49 H. Zhang, X. Zhang, C. Liu, S.-T. Lee and J. Jie, *ACS Nano*, 2016, **10**, 5113–5122.

50 L. Ye, H. Li, Z. Chen and J. Xu, *ACS Photonics*, 2016, **3**, 692–699.

51 M. B. Alemayehu, M. Falmbigl, K. Ta and D. C. Johnson, *ACS Nano*, 2015, **9**, 4427–4434.